A polyyne toxin produced by an antagonistic bacterium blinds and lyses a Chlamydomonad alga

Vivien Hotter[a], David Zopf[b,c,d,e], Hak Joong Kim[f], Anja Silge[b,c,d,e], Michael Schmitt[b,c], Prasad Aiyar[a], Johanna Fleck[b,c,d,e], Christian Matthäus[d], Julian Hniopek[b,c,d,e], Qing Yan[g], Joyce Loper[h], Severin Sasso[a,i], Christian Hertweck[f,j,1], Jürgen Popp[b,c,d,e,1], and Maria Mittag[a,1]

[a]Matthias Schleiden Institute of Genetics, Bioinformatics and Molecular Botany, Friedrich Schiller University Jena, 07743 Jena, Germany; [b]Institute of Physical Chemistry, Friedrich Schiller University Jena, 07743 Jena, Germany; [c]Abbe Center of Photonics, Friedrich Schiller University Jena, 07743 Jena, Germany; [d]Leibniz Institute of Photonic Technology, 07745 Jena, Germany; [e]Leibniz Research Alliance - Leibniz Health Technologies, 07745 Jena, Germany; [f]Department of Biomolecular Chemistry, Leibniz Institute for Natural Product Research and Infection Biology (HKI), 07745 Jena, Germany; [g]Department of Plant Sciences and Plant Pathology, Montana State University, Bozeman, MT 59717; [h]Department of Botany and Plant Pathology, Oregon State University, Corvallis, OR 97331; [i]Institute of Biology, Plant Physiology, Leipzig University, 04103 Leipzig, Germany; and [j]Faculty of Biological Sciences, Friedrich Schiller University Jena, 07743 Jena, Germany

Edited by David C. Baulcombe, University of Cambridge, Cambridge, United Kingdom, and approved June 22, 2021 (received for review April 23, 2021)

Algae are key contributors to global carbon fixation and form the basis of many food webs. In nature, their growth is often supported or suppressed by microorganisms. The bacterium *Pseudomonas protegens* Pf-5 arrests the growth of the green unicellular alga *Chlamydomonas reinhardtii*, deflagellates the alga by the cyclic lipopeptide orfamide A, and alters its morphology [P. Aiyar *et al.*, *Nat. Commun.* 8, 1756 (2017)]. Using a combination of Raman microspectroscopy, genome mining, and mutational analysis, we discovered a polyyne toxin, protegencin, which is secreted by *P. protegens*, penetrates the algal cells, and causes destruction of the carotenoids of their primitive visual system, the eyespot. Together with secreted orfamide A, protegencin thus prevents the phototactic behavior of *C. reinhardtii*. A mutant of *P. protegens* deficient in protegencin production does not affect growth or eyespot carotenoids of *C. reinhardtii*. Protegencin acts in a direct and destructive way by lysing and killing the algal cells. The toxic effect of protegencin is also observed in an eyeless mutant and with the colony-forming Chlorophyte alga *Gonium pectorale*. These data reveal a two-pronged molecular strategy involving a cyclic lipopeptide and a conjugated tetrayne used by bacteria to attack select Chlamydomonad algae. In conjunction with the bloom-forming activity of several chlorophytes and the presence of the *protegencin* gene cluster in over 50 different *Pseudomonas* genomes [A. J. Mullins *et al.*, bioRxiv [Preprint] (2021). https://www.biorxiv.org/content/10.1101/2021.03.05.433886v1 (Accessed 17 April 2021)], these data are highly relevant to ecological interactions between Chlorophyte algae and Pseudomonadales bacteria.

Chlamydomonas reinhardtii | eyespot | microbial interactions | *Pseudomonas* genome mining | Raman microspectroscopy

Cyanobacteria and algae in the aquatic environment contribute about 50% to global CO_2 fixation (1). As primary producers, they are fundamental to food webs (2, 3). Algal activities can also influence biogeochemical processes as exemplified recently with regards to the Greenland ice sheet (4). In nature, algae are usually associated with other microbes that influence their fitness through mutualistic or antagonistic interactions (3, 5, 6), and the exchange of natural products can play a central role in these interactions (7, 8). Despite their ecological importance, the interactions of algae with microorganisms are still poorly understood at the molecular level, especially relative to our understanding of higher plant–microbe interactions (8).

In recent years, the biciliate green alga *Chlamydomonas reinhardtii* (Fig. 1 *A* and *B*), for which a large molecular toolkit is available (9–11), has become a model for studying the molecular interactions between unicellular algae and microbes (7). *C. reinhardtii* occurs mainly in wet soil ecosystems (7) and can establish mutualistic carbon–nitrogen metabolic exchange mechanisms with fungi (12) or bacteria such as *Methylobacterium* spp (13). Moreover, algal–bacterial consortia have been used to mutualistically enhance natural hydrogen production of *C. reinhardtii* (14). However, *C. reinhardtii* can also be prone to attacks by antagonistic bacteria. For example, the soil bacterium *Streptomyces iranensis* releases the algicide azalomycin F, which is toxic for *C. reinhardtii* unless the alga protects itself among the mycelia of the fungus *Aspergillus nidulans* (15). In a previous study, we showed that another soil bacterium, *Pseudomonas protegens* Pf-5, known to produce a wide variety of secondary metabolites (16), can inhibit the growth of *C. reinhardtii* (17). Specifically, *P. protegens* Pf-5 releases orfamide A, a cyclic lipopeptide that causes a spike in cytosolic Ca^{2+} and rapid loss of cilia (historically known as flagella). However, an orfamide A–null mutant of *P. protegens* Pf-5 is still able to prevent *C. reinhardtii* cultures from growing for several days (17), leading us to hypothesize that at least another bacterial secondary metabolite is involved in the antagonism of *P. protegens* Pf-5 on *C. reinhardtii*. Here, we report the discovery of an unusual bacterial polyyne, protegencin, that plays a key role in the algicidal activity of *P. protegens* Pf-5: it causes destruction of the carotenoids within the eyespot, a primitive visual system (18, 19) (Fig. 1 *A* and *B*), and lysis of the algal cells.

Significance

Algae live in association with microbes that interact by a variety of chemical mediators, resulting in mutualistic or antagonistic relationships. Although algae are key contributors to carbon fixation and are fundamental for food webs, we still know little about the underlying molecular mechanisms affecting their fitness. This study investigates the interaction between an antagonistic bacterium and a unicellular alga. It demonstrates multiple roles of a polyyne, protegencin, that is used by the bacteria to attack green algal cells. It is a highly effective toxin that alters a subcellular algal compartment used for vision, bleaches, and lyses the algal cells. These results expand our knowledge of the arsenal of chemical mediators in bacteria and their modes of action in algal communities.

Author contributions: C.H., J.P., and M.M. designed research; V.H., D.Z., H.J.K., A.S., P.A., J.F., C.M., and J.H. performed research; V.H., D.Z., H.J.K., A.S., M.S., P.A., C.M., S.S., C.H., J.P., and M.M. analyzed data; V.H., D.Z., H.J.K., A.S., M.S., P.A., J.F., C.M., J.H., Q.Y., J.L., S.S., C.H., J.P., and M.M. wrote the paper; and Q.Y. and J.L. provided *hcnB* mutant.

The authors declare no competing interest.

This article is a PNAS Direct Submission.

[1]To whom correspondence may be addressed. Email: christian.hertweck@hki-jena.de, juergen.popp@ipht-jena.de, or m.mittag@uni-jena.de.

This article contains supporting information online at https://www.pnas.org/lookup/suppl/doi:10.1073/pnas.2107695118/-/DCSupplemental.

Published August 13, 2021.

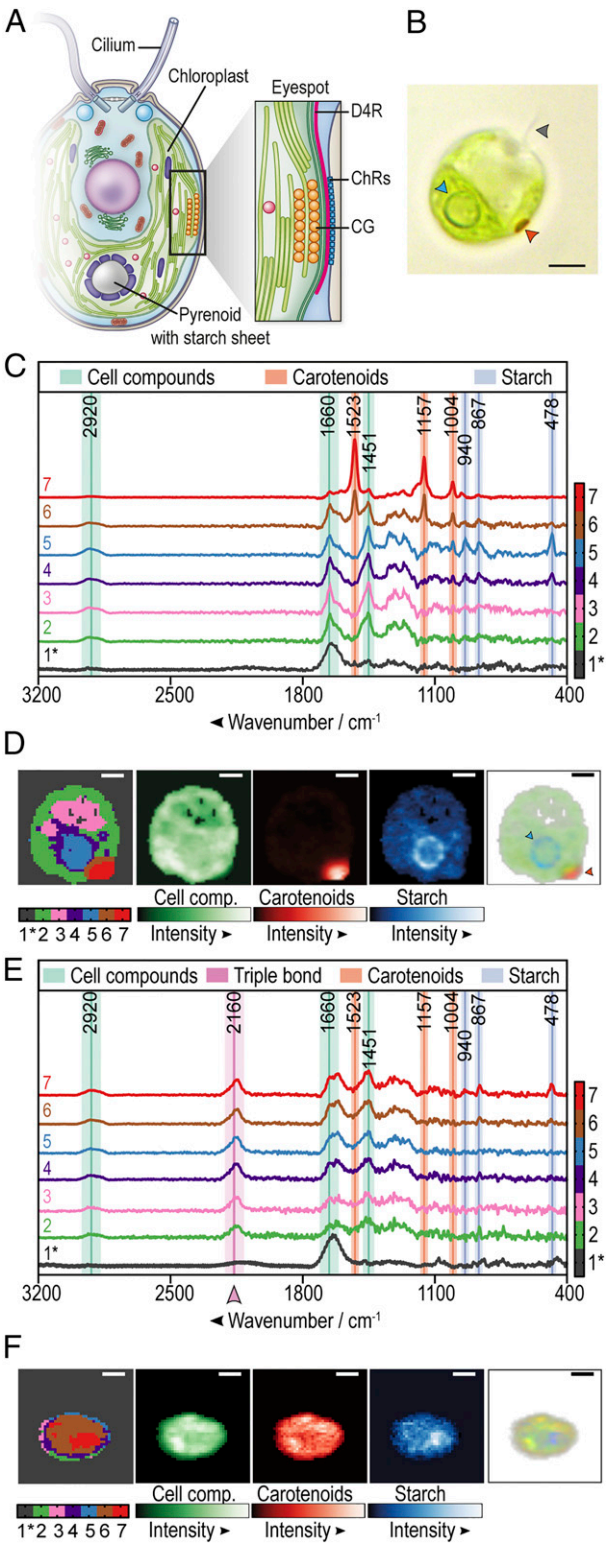

Fig. 1. Raman microspectroscopy of *C. reinhardtii* highlights the loss of eyespot carotenoids and an unidentified compound in bacterial coculture. (*A*) Simplified scheme of *C. reinhardtii* (modified from ref. 7, which is licensed under CC BY 4.0) with an enlarged eyespot area; data from (18, 19). CG, carotenoid-rich lipid globules; D4R, D4 rootlet; ChRs, channelrhodopsins. (*B*) Brightfield microscopic image of *C. reinhardtii*. The arrowheads highlight a cilium (gray), the pyrenoid (blue), and the eyespot (orange). (*C*) Raman spectroscopy of a representative *C. reinhardtii* cell grown in monoculture. An algal overnight culture in TAP was fixed with 4% formaldehyde and embedded in 0.5% TAP agarose for single cell analysis. The color-coded Raman spectra display the individual cluster spectra found by *k*-means cluster analysis of a typical algal cell. Raman marker bands are labeled green (cell compounds), blue (starch), and orange (carotenoids). Note that phenylalanine and carotenoids share a marker band at 1,004 cm^{-1} (*SI Appendix*, Table S1). The black spectrum (1*) represents the vector-normalized background generated from areas with low content of detectable biological material. All other displayed cluster spectra are background corrected and represent clusters of components rich in cell compounds (spectra 2 to 7), starch (spectra 4 and 5), or carotenoids (spectra 6 and 7). Additional spectra are shown in *SI Appendix*, Fig. S2. (*D*) Color-coded spatial distribution of Raman spectral components of a representative *C. reinhardtii* cell (*Left*) as shown in *C*. Green, orange, and blue false color maps represent Raman intensities of cell compounds, carotenoids, and starch, respectively. The composite red-green-blue (RGB) image (*Right*) is created by overlaying the normalized sums of the marker band regions associated with cell compounds (green), starch (blue), or carotenoids (red). The opacity in each pixel is proportional to the overall intensity in each pixel. The arrowheads highlight the starch sheets around the pyrenoid (blue) and the eyespot (orange). (*E*) Raman spectra of a representative *C. reinhardtii* cell after overnight cocultivation with *P. protegens* (algae:bacteria 1:1,000) in TAP medium. See *C* for further details. (*F*) Spatial distribution of the Raman spectroscopic clusters, integrated intensities and composite RGB image of a representative *C. reinhardtii* cell after overnight cocultivation with *P. protegens*. See *D* for details. (Scale bars: 3 μm in *B*, *D*, and *F*.) (*C*–*F*) Exemplary cells were taken from the 16-h series (Fig. 2*A*).

Results

Raman Microspectroscopy Detects Changes in Algal Eyespot Carotenoids and an Unexpected Compound in Algal–Bacterial Cocultures. To understand the antagonistic interplay between *C. reinhardtii* and *P. protegens* Pf-5 (hereafter referred to as *P. protegens*), we aimed to spatially resolve the molecular composition of algal samples in the absence and presence of the bacteria with subcellular resolution using Raman microspectroscopy (20). Due to the noninvasive nature of Raman microspectroscopy and the fact that water only mildly distorts Raman spectra, this technique is well suited to study biological samples (21) such as bacteria and unicellular algae (22–28), including *C. reinhardtii* (26–28).

Axenic algal cultures were first analyzed to establish a reference baseline for comparisons. To obtain efficient hyperspectral Raman images, *C. reinhardtii* cells were fixed in 4% formalin and embedded in 0.5% agarose to immobilize the cells (*SI Appendix*, Fig. S1); cells embedded solely in agarose were not sufficiently immobilized and were therefore not suitable for spatially resolved subcellular imaging. Raman images were recorded in the spectral range from 104 to 3,765 cm^{-1} using an excitation wavelength of 785 nm. Raman bands were assigned to relevant compounds according to characteristic wavenumbers listed in *SI Appendix*, Table S1. The spectral regions from 400 to 1,750 cm^{-1} and 2,800 to 3,200 cm^{-1} include typical marker bands for cell compounds (lipids and proteins), carotenoids, and starch (Fig. 1*C* and *SI Appendix*, Fig. S2). Raman intensity maps were calculated by the sum of intensities over specific compound marker bands in a spatially resolved manner (Fig. 1*D* and *SI Appendix*, Fig. S3). Two suborganelles were especially well visualized by Raman microspectroscopy: 1) the eyespot, based on its enriched carotenoids and 2) the pyrenoid, situated in the U-shaped chloroplast and detectable by its surrounding starch sheet layer (Fig. 1 *A* and *D*). It should be noted that the three-dimensional image of the cell within the agarose bed (*SI Appendix*, Fig. S1 and Fig. 1*D*) is projected in two-dimensions and thus the eyespot often appears to be localized nonhorizontally.

We then analyzed *C. reinhardtii* cells that were grown in coculture overnight with *P. protegens* Pf-5. Here, two major Raman spectroscopic changes were observed when compared with the spectra from axenic cultures (Fig. 1*C*): 1) algal cells showed strongly reduced peaks at wavenumbers 1,523, 1,157, and 1,004 cm^{-1}, which are all assigned to carotenoids (Fig. 1*E* and

SI Appendix, Fig. S2 and Table S1), and 2) a new peak appeared at ~2,160 cm^{-1}, which lies in the so-called "silent wavenumber region" for which there is no known overlap with Raman signatures of biological origin. This 2,160 cm^{-1} peak indicates the presence of a triple bond–containing compound (29). Interestingly, many *C. reinhardtii* cells examined in coculture with *P. protegens* had lost their typical eyespot carotenoids (Fig. 1*F*). To determine whether *P. protegens* produces the compound responsible for the peak in the silent wavenumber region, we performed Raman microspectroscopy on axenic bacterial cultures, which also showed a peak at ~2,150 cm^{-1} (*SI Appendix*, Fig. S4).

To study the appearance of the triple bond–bearing compound and the loss of eyespot carotenoids in bacterial–algal cocultures in greater detail, we incubated the *C. reinhardtii* cells with *P. protegens* for 16 and 24 h, using axenic algal cultures cultivated for the same periods of time as reference controls. In Fig. 2*A*, the carotenoid clusters are highlighted at 1,523, 1,157, and 1,004 cm^{-1}, although a typical protein marker band for phenylalanine is also detected at 1,004 cm^{-1} (30). The intensity ratio between 2,160 and 1,451 cm^{-1} (C-H deformation mode, the most prominent cell compound feature) was calculated as a measure for the presence of the triple-bond compound for each algal cell (Fig. 2*B*). These experiments confirmed that axenic algal cultures did not contain this compound and that it was only observed in coculture of *C. reinhardtii* with *P. protegens* (Fig. 2 *A* and *B*). Moreover, we observed a clear reduction in the number of carotenoid clusters in the presence of *P. protegens* (Fig. 2*B*). After 16 h in coculture, some algal cells appeared enlarged and the microscopically visible, yellow, carotenoid-rich lipid globules of the eyespot often disintegrated into smaller sized particles or were found to be absent as observed by brightfield microscopy (Fig. 2 *C* and *D* and *SI Appendix*, Fig. S5). After 24 h in coculture, algal cells appeared to lyse, and the eyespot carotenoids in most cells were undetectable (Fig. 2 *C* and *D* and *SI Appendix*, Fig. S5). Visualizing the spatial distribution of the triple-bond compound in algal cells cocultured with *P. protegens* for at least 16 h, we found that the substance sometimes accumulates in puncta but is also diffusely distributed throughout *C. reinhardtii* (*SI Appendix*, Fig. S6).

Two compounds containing triple bonds were known to be produced by *P. protegens*, hydrogen cyanide (16), and predicted polyyne(s) (31). The use of a *ΔhcnB* cyanide mutant JL4809 (16) in cocultures showed very similar observations as cocultures with wild-type *P. protegens* (*SI Appendix*, Fig. S7). Thus, hydrogen cyanide is not the relevant triple-bond compound.

Identification of the Polyyne Protegencin by Analytical Chemistry and Generation of a Protegencin-Null Mutant. Therefore, we considered polyynes, fatty acid derivatives with multiple C–C triple bonds, as alternatives. In bacteria, polyyne biosynthesis is encoded in gene clusters bearing genes for desaturases, a fatty acyl-AMP ligase, an acyl carrier protein, and a thioesterase (31). Mining the genome (32) of *P. protegens* revealed a tentative polyyne biosynthesis gene cluster (pgn) for a compound named "protegencin" (33). According to homology searches, *pgnE*, *pgnF*, and *pgnH* encode desaturases and a thioesterase; *pgnD* encodes a fatty acyl-AMP ligase, and *pgnG* encodes an acyl carrier protein (Fig. 3*A*). The predicted gene cluster includes genes PFL_0258 to PFL_0268, a previously identified orphan gene cluster with an unknown metabolic product (34). It is orthologous to the biosynthetic gene cluster for the polyyne "caryoynencin" [YP_257407-257414 (31)]. Parts of this gene cluster (PFL_0261-0267) are also homologous to a gene cluster for the biosynthesis of the polyynes "collimonins" produced by *Collimonas fungivorans* (35, 36). Thus, we predicted that *P. protegens* would produce at least one polyyne compound from the *pgn* gene cluster responsible for the Raman peak at 2,160 cm^{-1}. To test this, we created a targeted *pgn*-null mutant (*ΔpgnE*). Specifically, we inactivated the desaturase gene, *pgnE*, by means of a double-crossover knock-in strategy involving the introduction of an apramycin resistance gene (AprR) at the *pgnE* locus (*Materials and Methods* and Fig. 3 *A*–*C*).

By comparative high performance liquid chromatography (HPLC) analyses (photodiode array [PDA] 220 to 400 nm) of ethyl acetate extracts of wild-type and *ΔpgnE* mutant *P. protegens* cultures grown in TAP (Tris-Acetate-Phosphate) medium (Fig. 3*D* and *SI Appendix*, Fig. S8), we detected a candidate polyyne compound with a characteristic ultraviolet signature. We successfully isolated this compound, protegencin, and elucidated its structure using high-resolution mass spectrometry (MS) and NMR spectroscopic analysis (Fig. 3*E* and *SI Appendix*, Figs. S8–S13 and Table S2). Protegencin is a highly unsaturated octadecanoid fatty acid with four conjugated triple bonds and one double bond. A copper-catalyzed alkyne–azide cycloaddition (CuAAC) reaction with benzyl azide confirmed that this compound has a reactive terminal triple bond (Fig. 3 *D* and *E* and *SI Appendix*, Fig. S8). Metabolic profiling of the verified *ΔpgnE* mutant (Fig. 3*C*) showed that protegencin production was completely abolished (Fig. 3*D*).

Protegencin Causes the Disappearance of Eyespot Carotenoids in Coculture. In *C. reinhardtii* cocultures with the *ΔpgnE* mutant, the 2,160-cm^{-1} Raman peak was absent (Fig. 3 *F* and *G*), consistent with the lack of expressed protegencin. We confirmed that protegencin is responsible for the 2,160 cm^{-1} Raman peak by predicting its Raman spectrum by means of density functional theory (DFT). DFT calculations predicted characteristic features between 2,100 and 2,200 cm^{-1}, in good agreement with empirically observed peak features (*SI Appendix*, Fig. S4).

We observed that eyespot carotenoid clusters in *C. reinhardtii* were not affected by coculture with the *ΔpgnE* mutant strain (Fig. 3*G*). These findings suggest that protegencin is the cause for the disappearance of the algal eyespot carotenoid clusters. Consistent with this, after 16 h in coculture with the *ΔpgnE* mutant, a single eyespot was visible in most *C. reinhardtii* cells by brightfield microscopy; after 24 h in coculture, some algal cells had a single eyespot, while others displayed several well visible carotenoid-rich structures (Fig. 3 *H* and *I* and *SI Appendix*, Fig. S5). In the absence of protegencin expression, *C. reinhardtii* eyespot carotenoids were not degraded in coculture with *P. protegens*.

Protegencin Lyses and Kills Chlorophyte Algae, but the Eyespot Is not a Prerequisite for its Toxic Activity. To corroborate the role of protegencin in algal killing, we evaluated the direct effect of purified compound on *C. reinhardtii* cells, focusing on the integrity of the algal cell membrane as assayed by Evans blue dye exclusion. Mastoparan, a toxin from wasp venom known to cause lysis and death of *C. reinhardtii*, was used as a positive control at a concentration of 10 μM (37). In the presence of mastoparan, about 90% of the cells of *C. reinhardtii* were stained with Evans blue after 30 s (*SI Appendix*, Fig. S14). Protegencin, which was dissolved in dimethyl sulfoxide (DMSO) after its purification (*SI Appendix*, *SI Methods*), was used at a similar concentration (2% vol/vol equivalent to 10.4 μM), as determined by the Click reaction and HPLC analysis (*Materials and Methods*). Protegencin treatment resulted in Evans blue staining of >95% of the cells after 24 h of incubation (*SI Appendix*, Fig. S14). This experiment was repeated with a lower concentration of protegencin (0.5% vol/vol), which had the same effect (Fig. 4*A*). These data show that protegencin can efficiently perforate *C. reinhardtii* cell membranes even at low micromolar concentrations. We also evaluated the toxicity of protegencin on *C. reinhardtii* after short incubation with 0.5% vol/vol protegencin by survival assays (modified from ref. 38). Incubation with protegencin for only 1 h reduced colony-forming units (CFUs; visible after 7 d) down to about 10% (*SI Appendix*, Fig. S15); an incubation time of 4 h resulted in no CFUs (Fig. 4*B*), supporting the highly toxic effect of protegencin on *C. reinhardtii*.

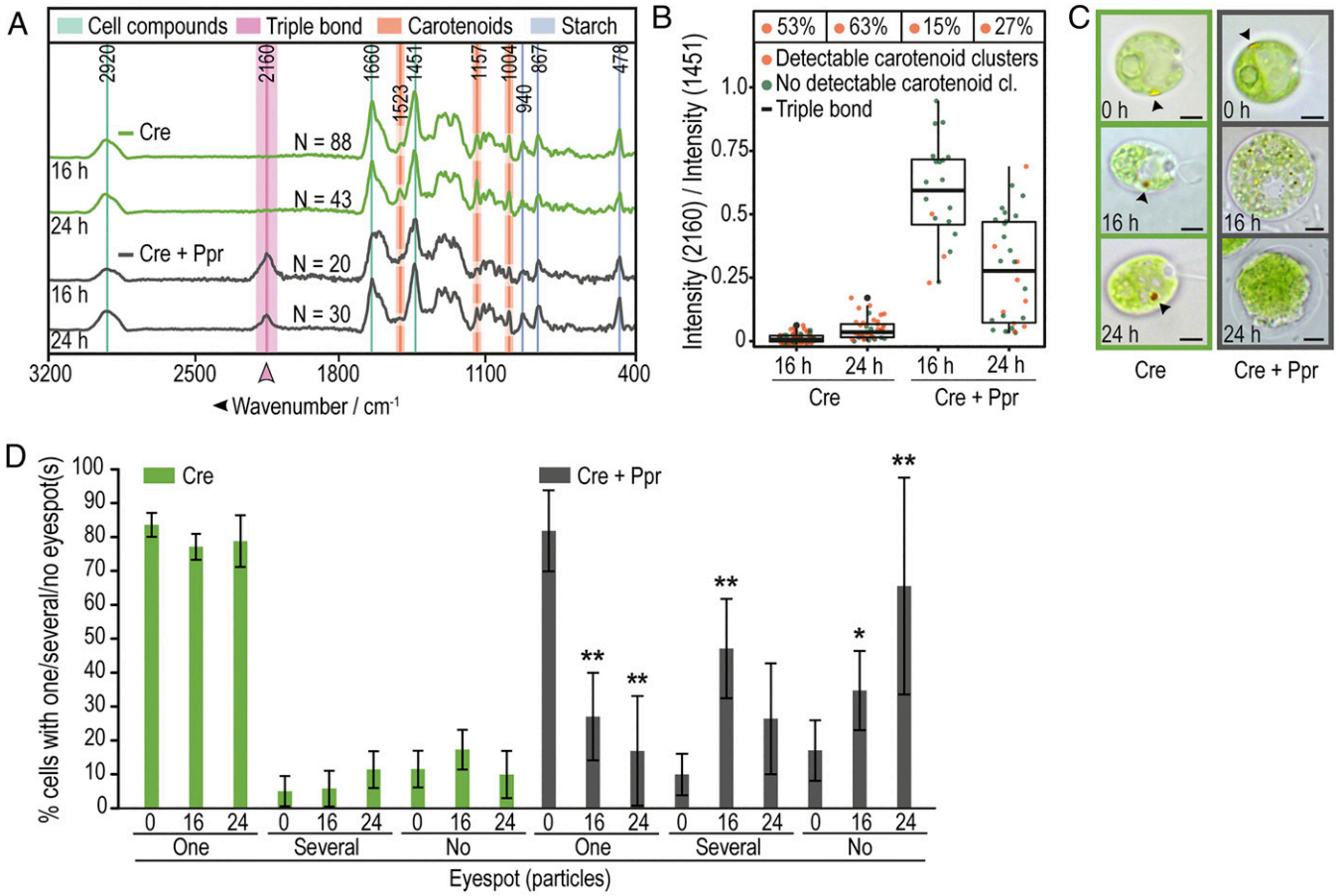

Fig. 2. Disappearance of eyespot carotenoids coincides with the appearance of a triple bond–containing compound (TC). (*A*) Average Raman spectra of *C. reinhardtii* show a peak at 2,160 cm^{-1} and reduction of detectable carotenoid peaks over time when cocultured with *P. protegens* (Cre + Ppr) compared with axenic *C. reinhardtii* (Cre). Cultures were grown for 16 or 24 h in TAP. Spectra of algal cells were generated by averaging over all pixels for the relevant Raman spectral class within the cell body. *n* = total number of analyzed cells. All data were obtained from at least three independent experiments. (*B*) Summary of Raman spectroscopic measurements from (*A*) show the presence of the TC (box plot) and a reduction of carotenoid clusters in cocultures (Cre + Ppr). The data points plotted are for the ratio of average Raman intensities associated with the TC (2,160 cm^{-1}) versus a dominant band representing *C. reinhardtii* cellular material (C-H deformation mode at 1,451 cm^{-1}). Each point represents a measurement of a single alga; box plots indicate quartiles; % values above each box summarize the fraction of cells with detected carotenoid cluster(s). (*C*) Representative brightfield microscopic images of axenic *C. reinhardtii* (green) and in coculture (*C*, Cre + Ppr, gray) after 0, 16, or 24 h show the disappearance of eyespots as visualized by their carotenoids (see arrowhead) over time in the presence of bacteria. (Scale bars: 3 μm.) Further cells are shown in *SI Appendix*, Fig. S5. (*D*) Fraction of algal cells (from *A*–*C*) with visible eyespots as determined by brightfield microscopy. After 16 h in coculture, the eyespot is mostly disintegrated and undetectable based on its color after 24 h, whereas most cells in the axenic culture maintain one eyespot. The asterisks indicate significant differences as calculated by the Kruskal–Wallis test with Dunn's post hoc test (*$P < 0.05$; **$P < 0.01$) in coculture compared with axenic *C. reinhardtii* at the same time point. The error bars indicate SDs with $n \geq 300$ cells per time point and culture.

As the effect of protegencin includes destruction of the eyespot carotenoids, we examined whether an eyeless mutant strain, *eye3-2* (CC-4316), could be lysed with protegencin; this mutant has a defect in forming eyespot globule layers (39) and was lysed at similar rates (Fig. 4 *A* and *B*) as the mutant's background strain CC-125 (Fig. 4*A*). These data show that the protegencin-mediated mechanism of algal cell lysis does not require destruction of the eyespot carotenoids. We were also interested in finding out if protegencin acts specifically on *C. reinhardtii* or whether it may also harm other algae. We examined its effect on the Chlorophyte alga *Gonium pectorale*, a colony-forming green alga, and showed that it too can be lysed and killed by protegencin (Fig. 4 *A* and *B*).

Protegencin Is the Major Algicidal Toxic Metabolite of *P. protegens*. To test whether protegencin is the primary metabolite causing growth arrest and bleaching of algal cells, we compared coculture growth of *C. reinhardtii* with *P. protegens* wild-type, *ΔhcnB* cyanide mutant, or *ΔpgnE* mutant strains over a period of 7 d (Fig. 4*C* and *SI Appendix*, Fig. S16). Axenic *C. reinhardtii* cultures were used as controls (Fig. 4*C* and *SI Appendix*, Fig. S16). As observed previously (17), *C. reinhardtii* cells do not grow in coculture with *P. protegens*. The characteristic chlorophyll-green color of algal monocultures is absent in cocultures due to growth arrest [Fig. 4*C* and *SI Appendix*, Fig. S16*C* (17)]. In coculture with the *ΔhcnB P. protegens* cyanide mutant, no algal growth is visible either. In contrast, algal cells grow well in coculture with the *ΔpgnE* protegencin mutant (Fig. 4 *C*, *Right*, and *SI Appendix*, Fig. S16*C*). These findings corroborate that protegencin is a major toxin secreted by *P. protegens* against *C. reinhardtii* and, in conjunction with orfamide A that prevents the escape of the algal cells by deflagellation (Fig. 4*D*), is part of a powerful bacterial attack strategy.

Discussion

Although algae are key contributors to global carbon fixation and fundamental to food webs, how they interact with microbes is still not well understood. Recently, several studies on algicidal bacteria and their natural products have been reported (reviewed in ref. 3) that have provided the first insights into these algicidal

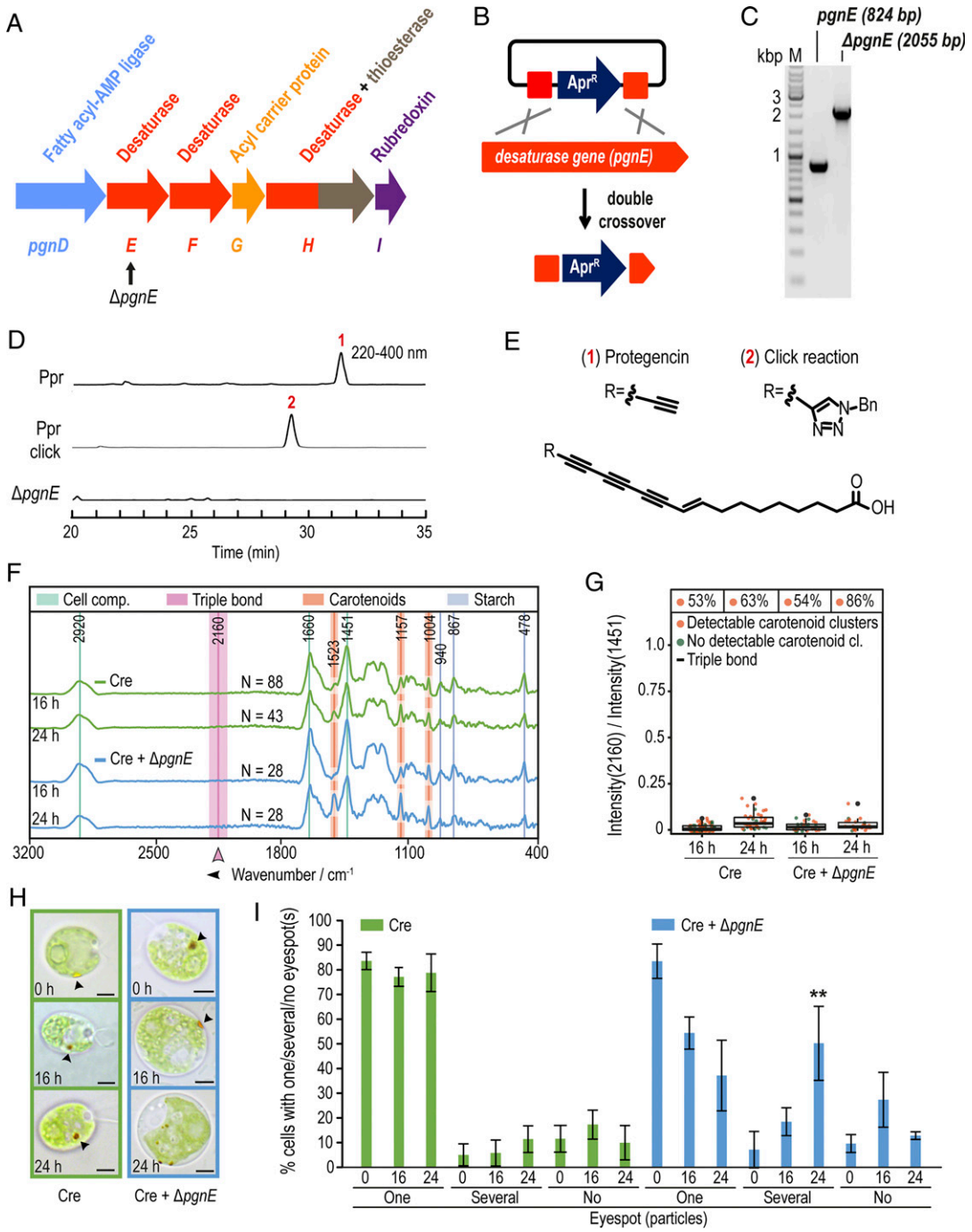

Fig. 3. Identification of protegencin in cocultures using a *P. protegens* mutant deficient in protegencin production and its effects on carotenoid clusters. (*A*) *Protegencin* (*pgn*) biosynthesis gene cluster (PFL_0261-0266) with knock-out target gene, *pgnE*, indicated (PFL_0262, black arrow). (*B*) Double crossover strategy used to obtain a *P. protegens* mutant deficient in protegencin production. (*C*) Agarose gel shows successful insertion of the *Apr* gene in *pgnE*. (*D*) HPLC analysis (PDA 220 to 400 nm) of *P. protegens* culture extracts, Click reaction product, and of *ΔpgnE* mutant extracts. (*E*) Structure of protegencin as determined from NMR and high-resolution MS analysis (*SI Appendix*, Figs. S8–S13); Bn, Benzyl. (*D* and *E*) Experiments were repeated at least three times. (*F*) Raman spectroscopy of axenic *C. reinhardtii* (green, Cre) and in coculture with the *P. protegens pgnE*-null mutant (Cre + *ΔpgnE*, light blue) suggests that protegencin is the compound responsible for the peak at 2,160 cm^{-1}, which remains absent even after 24 h of coculturing (n = total number of analyzed cells). All data were obtained from at least three independent experiments. See legend of Fig. 2*A* for further details. (*G*) Summary of Raman spectroscopic measurements presented in *A*, with % *Above* each box representing the total fractions of algal cells with carotenoid cluster(s). See legend of Fig. 2*B* for further details. (*H*) Representative brightfield micrographs of axenic *C. reinhardtii* (green) and in coculture with the *P. protegens ΔpgnE*-null mutant (blue) after 0, 16, or 24 h show that the eyespot disintegrates slower than in cocultures with *P. protegens* wild-type or *ΔhcnB* mutant strains (see Fig. 2 *C* and *D*; arrowheads highlight the eyespot; scale bars: 3 μm). Further micrographs are shown in *SI Appendix*, Fig. S5. (*I*) Fraction of algal cells with visible eyespots as determined by brightfield microscopy of cultures analyzed in (*F*–*H*) after 0, 16, and 24 h. After 16 h in coculture, the eyespot is mostly still present; after 24 h, it disintegrates in more than one eyespot in about one-half of the cells. Asterisks indicate significant differences as calculated by the Kruskal–Wallis test with Dunn's post hoc test (*$P < 0.05$; **$P < 0.01$; and ***$P < 0.001$) in coculture compared with axenic *C. reinhardtii* at the same time point. The error bars indicate SDs with $n \geq 300$ cells per time point and culture.

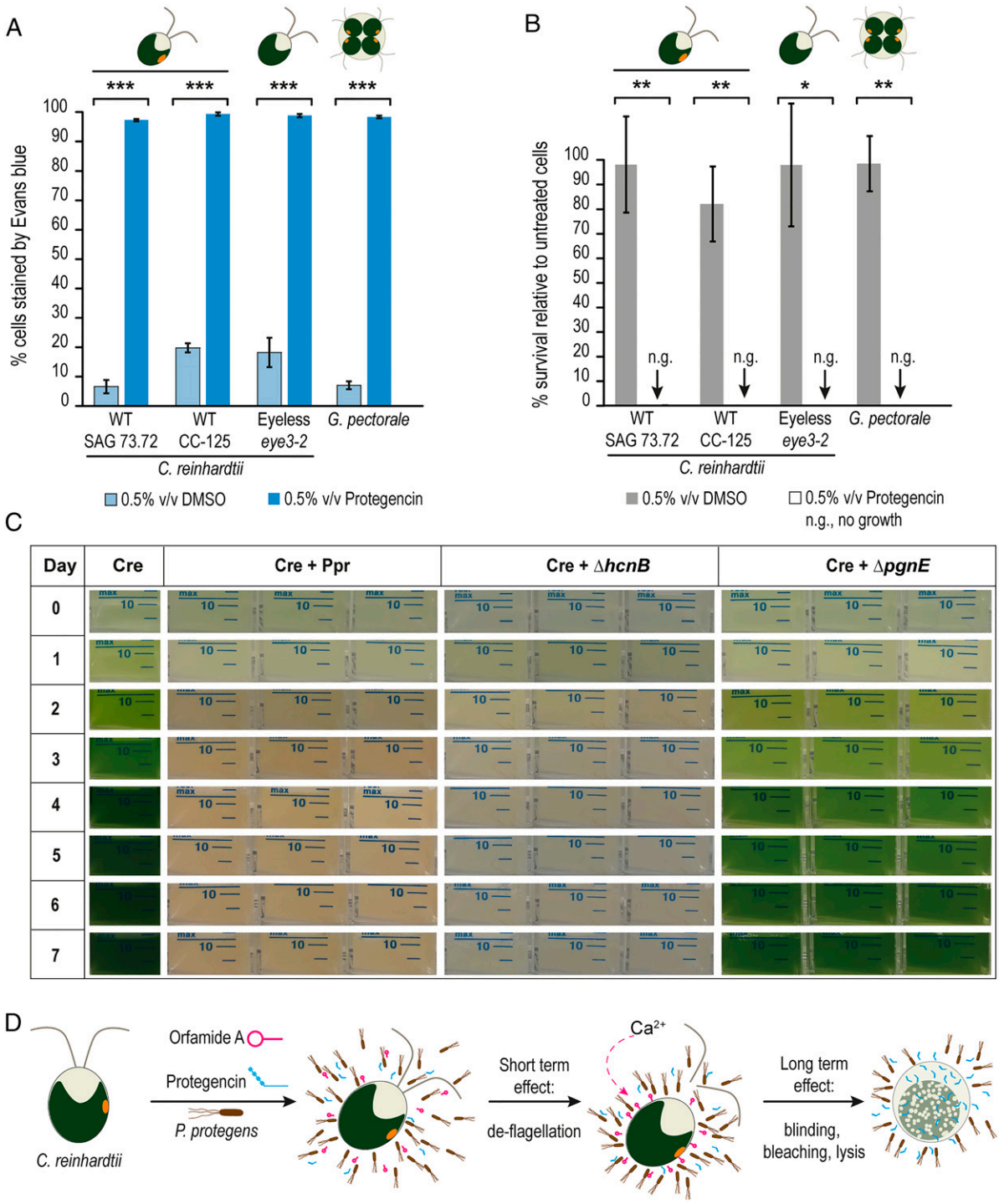

Fig. 4. Protegencin, a potent toxin for select Chlamydomonad algae that lyses and bleaches them. (*A*) Protegencin effectively damages the cell membrane of *C. reinhardtii*, of its eyeless mutant *eye3-2* and of the colony-forming *G. pectorale* after 24 h of incubation as evaluated by Evans blue staining. As negative control, DMSO (solvent for protegencin) was used and as control for the *eye3-2* mutant; its background strain CC-125 (*Materials and Methods*) was included. For each treatment, three independent replicates with three technical replicates each were examined; for each technical replicate per time point and treatment, $n \geq 500$ cells were analyzed. (*B*) After 4 h of incubation with 0.5% (vol/vol) purified protegencin, cells of *C. reinhardtii*, its *eye3-2* mutant, and of *G. pectorale* do not survive after several days. Controls, DMSO and strain CC-125; n.g., no growth. For detailed experimental procedures, see *SI Appendix, SI Methods*. For each treatment, three independent replicates with three technical replicates each were examined. The error bars indicate SDs and asterisks indicate significant differences, calculated by Student's *t* test (*$P < 0.05$; **$P < 0.01$; and ***$P < 0.001$). (*C*) In liquid cocultures of *C. reinhardtii* with *P. protegens*, *ΔhcnB*, or *ΔpgnE* mutants, algal growth is only possible when protegencin production is prevented. Experiments were conducted three times independently, each with three technical replicates. (*D*) Proposed scheme of *P. protegens*' algicidal activity toward *C. reinhardtii*. Harmful secondary metabolites orfamide A (magenta) and protegencin (cyan) are produced by *P. protegens*. Orfamide A triggers an increase in cytosolic Ca^{2+} that results in deflagellation of the algae within minutes (17). Slower (on the order of hours), more potent damage by protegencin resulting in eyespot decay ("blinding"), bleaching, and algal cell lysis occurs subsequently.

mechanisms. Studies involving in situ chemical analysis of microbial interactions and/or genetic manipulations to alter the production of the bacterial secondary metabolites to test the basis for interaction are still rare.

Here, we identified and characterized a natural product underlying an antagonistic interaction between the green unicellular alga *C. reinhardtii* and the bacterium *P. protegens*, both soil organisms that are genetically tractable models for laboratory conditions, enabling the study of their interaction in a controlled environment. Using genetically constructed mutants, brightfield microscopy, label-free Raman microspectroscopy, high-resolution MS, and NMR analyses, we discovered an unusual bacterial toxin, the polyyne protegencin, which causes destruction of the eyespot carotenoids and algal cell lysis. In the future, the role of protegencin in interactions between *C. reinhardtii* and *P. protegens* should be evaluated in more natural conditions, in addition to the standardized conditions evaluated in this study.

P. protegens produces a variety of secondary metabolites controlled by the GacS-GacA regulatory system (16, 34, 40), including the *pgn* cluster. The production of a polyyne was predicted in silico (31) and recently verified in *Pseudomonas* (33, *SI Appendix*, *SI Note*). Polyynes like protegencin are notoriously unstable compounds. They have been isolated from different organisms, including a variety of land plants, fungi, and insects. However, few bacterial polyynes are known to be of ecological relevance (31, 41–43). The first identified bacterial gene cluster coding for the biosynthesis of a polyyne was caryoynencin from *Burkholderia* spp (31). In a previous genome mining analysis, orthologous *pgn* gene clusters were also found in *Collimonas* and *Mycobacterium* as well as in different *Burkholderia* species (31). Recently, the distribution of the *pgn* cluster was found in over 50 different *Pseudomonas* genomes (33). Currently, it is not known whether all these bacteria can also exert algicidal activities using polyynes; the interactions of these bacteria have also only been studied with organisms other than photosynthetic protists. Some bacterial polyynes have been shown to provide protection for other organisms [e.g., the polyyne caryoynencin is part of a blend of antibiotics produced by symbiotic *Burkholderia gladioli* bacteria to protect the egg stage of a group of herbivorous beetles against detrimental bacteria (44)]. Cepacin, from *Burkholderia ambifaria*, is used as a biocontrol agent to protect the garden pea *Pisum sativum* from attack by oomycetes (45). Cepacin A and B, isolated from *Pseudomonas cepacia*, exert activities against other microbes [e.g., Staphylococci (46)]. The polyyne collimomycin, later renamed to collimonin, from the mycophagous bacterium *C. fungivorans* inhibits the growth of *Aspergillus niger* hyphae and controls hyphal branching and pigmentation (35, 36). In contrast, protegencin characterized in this study plays an unprecedented role as a potent bacterial toxin against the green alga *C. reinhardtii*.

Previously, we have shown that another *P. protegens* natural product, orfamide A, immobilizes select Chlorophyte algae (17). Orfamide A triggers an increase in cytosolic Ca^{2+} but is unable to penetrate the algal cells even at a concentration of 35 μM within 30 s (17). In contrast, protegencin permeates *C. reinhardtii* cells by affecting the integrity of the cell membrane in a yet-unknown manner and kills them. This is also true for cells of the colony-forming Chlorophyte *G. pectorale,* which lives in ponds and belongs to the same algal order of *Chlamydomonadales*, formerly known as *Volvocales* (Fig. 4 *A* and *B*). This knowledge is also of high ecological relevance as colony-forming *Chlamydomonadales* can form algal blooms (47, 48), and some *Pseudomonas* species are known to control such blooms (49).

The two algicidal toxins orfamide A and protegencin from *P. protegens* have complementary activities; they are not only chemically different but also functionally distinct. Orfamide A can rapidly deflagellate algal cells (17). Considering the timescale for the action of the two compounds, these bacteria may use a two-step strategy to antagonize algae: 1) quick immobilization (deflagellation) of algal cells by orfamide A, followed by 2) an artillery-like attack using polyynes such as protegencin whereby the cells are lysed (Fig. 4*D*). The destruction of eyespot carotenoids in algal cells, leaving them effectively "blind", may be an early-intermediate strategy to disorient the alga and allow time for lysis before they can (phototactically) escape. If the chemical compound, orfamide A, gets depleted, cilia could be restored in 1 to 2 h (50). The eyespot is a primitive visual system consisting of carotenoid-filled pigment granules subtended by thylakoid membranes; these layers have the function of a quarter-wave plate (18). It allows the algae to detect the direction as well as the intensity of the light and thus controls their phototactic behavior (18, 19). In a mutant that is not able to produce carotenoids, such as the *lts2-204* mutant, which is defective in the first enzyme of carotenoid biosynthesis (phytoene synthase), the eyespot structure is disordered and its position mislocalized; also, other subcellular compartments are affected. The mutant shows neither positive nor negative phototaxis (51).

In their natural habitats, algae interact with microbes via a variety of chemical mediators, resulting in mutualistic or antagonistic relationships. This study sheds light on the chemical weapons used by antagonistic bacteria and their modes of action in algal communities. It reveals fundamental mechanisms for how fitness of photosynthetic microbes can be influenced and specifically the role and mode of action of polyynes in the arsenal of algicidal bacteria.

Materials and Methods

Strains and Culture Conditions. *C. reinhardtii* strain SAG 73.72 (mt^+), obtained from the algal culture collection in Göttingen, was used for all experiments. It is also known as CC-3348. In addition, the following algae were used for Evans blue staining and survival assays: *C. reinhardtii* strain CC-125, also known as 137c (*nit1*, *nit2*, *agg1*$^+$, mt^+), was used as the background strain for the *eye3-2* mutant CC-4316 (39) and *G. pectorale* strain CCAP 32/4, obtained from the culture collection of algae and protozoa of the Scottish Marine Institute. *C. reinhardtii* was grown in liquid TAP medium (50) at 23 °C under a 12:12 light–dark cycle under white light (Osram L36W/840, lumilux, cool white, Osram) with a light intensity of 55 μmol · m^{-2} · s^{-1} and constant orbital shaking (100 rpm). *G. pectorale* was grown under the same conditions in the medium suggested by the culture collection, 3N-BBM + V medium. *P. protegens* strain Pf-5 was used as bacterial wild type (52). A cyanide mutant, *ΔhcnB* mutant, JL4809 (16), was used as well as a Pf-5 strain deficient in protegencin production (see *Creation of a* P. protegens *Protegencin Mutant*), *ΔpgnE*. Axenic bacteria were grown in Luria-Bertani (LB) medium at 28 °C with constant orbital shaking (200 rpm) or in TAP medium, as stated.

Algal Bacterial Cocultures. For the cocultures, *C. reinhardtii* CC-3348 cells were precultured to a cell density of 3 to 6 × 10^6 cells · mL^{-1}. Bacterial precultures were grown to an optical density $OD_{600} > 4$ (as determined by serial dilutions of the bacterial precultures) overnight. Prior to cocultivation, bacterial cells were washed twice with TAP medium. All cells were then reinoculated in TAP medium with a starting algal cell density of 2 × 10^5 cells · mL^{-1} and a bacterial cell density of 2 × 10^8 cells · mL^{-1}. The cocultures were grown under the conditions mentioned above for the growth of *C. reinhardtii*. As control, axenic *C. reinhardtii* cultures were inoculated at a starting cell density of 2 × 10^5 cells · mL^{-1} and grown and analyzed accordingly.

Creation of a *P. protegens* Protegencin Mutant. To inactivate the gene *pgnE* of the protegencin gene cluster of *P. protegens*, a target double crossover strategy was chosen to insert the apramycin resistance gene from PIJ773 into each cay gene. Details are presented in *SI Appendix*, *SI Methods*.

Sample Preparation for Raman Imaging. Axenic *C. reinhardtii* and cocultures of *C. reinhardtii* with *P. protegens* wild type and mutants were grown as mentioned in *Strains and Culture Conditions* and in *Algal Bacterial Cocultures*. An aliquot of cell suspension (1.5 mL) was removed under sterile conditions, fixed in 4% (vol/vol) formalin for 10 min, and centrifuged for 5 min at 4,500 × *g*. Afterward, the supernatant was removed, and the cell pellet was resuspended in 375 μL TAP. The obtained suspension was mixed with 375 μL hand warm 1% (wt/vol) agarose in TAP. The agarose–cell mixture was quickly transferred onto CaF_2 substrate and cooled down at 4 °C for at least 15 min. The sample substrates were covered with distilled water before Raman measurements.

Hyperspectral Raman Imaging. Hyperspectral Raman images were acquired using a confocal Raman imaging microscope (alpha 300 R, WITec) with a water immersion objective (Nikon Corporation; magnification: 60×; numerical aperture: 1.0). The excitation light with a wavelength of 785 nm was provided by a cw diode laser (Toptica Photonics). The waist diameter of the confocal volume was estimated by calculating the diameter of the central Airy disk and is ∼0.96 μm ($d_{Airy} = 1.22\ \lambda_{Laser}/NA_{Objective}$; λ_{Laser} = 785 nm, $NA_{Objective}$ = 1.0). The excitation power measured at the front lens of the objective was ∼70 mW. Raman scattered light was dispersed by a diffraction grating (300 grooves · mm^{-1}) and detected by a cooled electron multiplying charge-coupled device detector in a range from 104 to 3,765 cm^{-1}. Algal samples were selected under the microscope, and single algal cells were centered in a 15 × 15 μm large *x*,*y*–scanning grid. The hyperspectral Raman data cube was generated by point-wise integration of the scanning grid in *x*- and *y*-direction with a step-size of 0.34 μm equal in both spatial directions. Two independent scans of the area incorporating a single algal cell were performed. In an initial rapid scan (integration time: 100 ms/pixel), the autofluorescence of the algae was bleached to decrease the background fluorescence level. The subsequent acquisition scan was performed with a dwell time of 500 ms/pixel and a hyperspectral data cube I (x, y, ν) with the dimension of 45 × 45 pixel × 1,024 wavenumbers was obtained.

Preprocessing of the Raman Spectra. All raw data were processed and analyzed by an in-house–developed script in the programming language R (version 4.0.2) (53). The preprocessing is described in detail in refs. 54 and 55. In short, the Raman spectra were cleared from cosmic spikes and wavenumber calibration was performed with 4-acetaminophenol. Subsequently, the wavenumber region was restricted to 350 to 3,300 cm^{-1}. The wavenumber axis of all spectra was interpolated using a cubic fmm-spline (new wavenumber pitch: 3 cm^{-1}) and background corrected by employing a statistic-sensitive nonlinear iterative peak–clipping algorithm (smoothing = true, iteration = 100, window = "3") (56). To minimize the influence of the agarose embedding on Raman algal cell spectra, an additional correction was performed accounting for the spectral influence of the agarose (see *SI Appendix* for computational details).

Data Availability. All study data are included in the article and/or *SI Appendix*.

ACKNOWLEDGMENTS. We thank Erik Hom and Jakob Sprague for proofreading the manuscript and for constructive comments on the manuscript, Georg Kreimer for helpful comments on Fig. 1*A*, and Debbie Maizels for its design. Our work was supported by fellowships from the International Leibniz Research School, abbreviated as ILRS (under the head of the Jena School for Microbial Communication) awarded to V.H., and P.A., D.Z., A.S., S.S., C.H., J.P., and M.M. were funded by the Deutsche Forschungsgemeinschaft (German Research Foundation) by grant Sonderforschungsbereich (SFB) 1127/2 ChemBioSys 239748522.

1. C. B. Field, M. J. Behrenfeld, J. T. Randerson, P. Falkowski, Primary production of the biosphere: Integrating terrestrial and oceanic components. *Science* **281**, 237–240 (1998).
2. J. H. Steele, "Marine food webs" in *The Structure of Marine Ecosystems*, J. H. Steele, Ed. (Harvard University Press, 1974), pp. 9–28.
3. N. Meyer, A. Bigalke, A. Kaulfuß, G. Pohnert, Strategies and ecological roles of algicidal bacteria. *FEMS Microbiol. Rev.* **41**, 880–899 (2017).
4. J. McCutcheon *et al*., Mineral phosphorus drives glacier algal blooms on the Greenland Ice Sheet. *Nat. Commun.* **12**, 570 (2021).
5. E. Cirri, G. Pohnert, Algae-bacteria interactions that balance the planktonic microbiome. *New Phytol.* **223**, 100–106 (2019).
6. M. B. Cooper, A. G. Smith, Exploring mutualistic interactions between microalgae and bacteria in the omics age. *Curr. Opin. Plant Biol.* **26**, 147–153 (2015).
7. S. Sasso, H. Stibor, M. Mittag, A. R. Grossman, From molecular manipulation of domesticated *Chlamydomonas reinhardtii* to survival in nature. *eLife* **7**, e39233 (2018).
8. E. F. Y. Hom, P. Aiyar, D. Schaeme, M. Mittag, S. Sasso, A chemical perspective on microalgal–microbial interactions. *Trends Plant Sci.* **20**, 689–693 (2015).
9. I. K. Blaby *et al*., The *Chlamydomonas* genome project: A decade on. *Trends Plant Sci.* **19**, 672–680 (2014).
10. P. A. Salomé, S. S. Merchant, A series of fortunate events: Introducing *Chlamydomonas* as a reference organism. *Plant Cell* **31**, 1682–1707 (2019).
11. M. Schroda, Good news for nuclear transgene expression in *Chlamydomonas*. *Cells* **8**, 1534 (2019).
12. E. F. Y. Hom, A. W. Murray, Plant-fungal ecology. Niche engineering demonstrates a latent capacity for fungal-algal mutualism. *Science* **345**, 94–98 (2014).
13. V. Calatrava, E. F. Y. Hom, Á. Llamas, E. Fernández, A. Galván, OK, thanks! A new mutualism between *Chlamydomonas* and methylobacteria facilitates growth on amino acids and peptides. *FEMS Microbiol. Lett.* **365**, fny021 (2018).
14. N. Fakhimi, D. Gonzalez-Ballester, E. Fernández, A. Galván, A. Dubini, Algae-bacteria consortia as a strategy to enhance H_2 production. *Cells* **9**, 1353 (2020).
15. M. K. C. Krespach *et al*., Lichen-like association of *Chlamydomonas reinhardtii* and *Aspergillus nidulans* protects algal cells from bacteria. *ISME J.* **14**, 2794–2805 (2020).
16. J. E. Loper *et al*., Comparative genomics of plant-associated *Pseudomonas* spp.: Insights into diversity and inheritance of traits involved in multitrophic interactions. *PLoS Genet.* **8**, e1002784 (2012).
17. P. Aiyar *et al*., Antagonistic bacteria disrupt calcium homeostasis and immobilize algal cells. *Nat. Commun.* **8**, 1756 (2017).
18. C. L. Dieckmann, Eyespot placement and assembly in the green alga *Chlamydomonas*. *BioEssays* **25**, 410–416 (2003).
19. M. Schmidt *et al*., Proteomic analysis of the eyespot of *Chlamydomonas reinhardtii* provides novel insights into its components and tactic movements. *Plant Cell* **18**, 1908–1930 (2006).
20. B. Kann, H. L. Offerhaus, M. Windbergs, C. Otto, Raman microscopy for cellular investigations – From single cell imaging to drug carrier uptake visualization. *Adv. Drug Deliv. Rev.* **89**, 71–90 (2015).
21. C. Krafft *et al*., Label-free molecular imaging of biological cells and tissues by linear and nonlinear Raman spectroscopic approaches. *Angew. Chem. Int. Ed. Engl.* **56**, 4392–4430 (2017).
22. B. Lorenz, C. Wichmann, S. Stöckel, P. Rösch, J. Popp, Cultivation-free Raman spectroscopic investigations of bacteria. *Trends Microbiol.* **25**, 413–424 (2017).
23. N. Parab, V. Tomar, Raman spectroscopy of algae: A review. *J. Nanomed. Nanotechnol.* **3**, 24 (2012).
24. M. Hosokawa *et al*., In vivo live cell imaging for the quantitative monitoring of lipids by using Raman microspectroscopy. *Anal. Chem.* **86**, 8224–8230 (2014).
25. T. Wang *et al*., Quantitative dynamics of triacylglycerol accumulation in microalgae populations at single-cell resolution revealed by Raman microspectroscopy. *Biotechnol. Biofuels* **7**, 58 (2014).
26. S. K. Sharma *et al*., An integrative Raman microscopy-based workflow for rapid in situ analysis of microalgal lipid bodies. *Biotechnol. Biofuels* **8**, 164 (2015).
27. Y. Kubo, T. Ikeda, S. Y. Yang, M. Tsuboi, Orientation of carotenoid molecules in the eyespot of alga: In situ polarized resonance Raman spectroscopy. *Appl. Spectrosc.* **54**, 1114–1119 (2000).
28. H. Wu *et al*., In vivo lipidomics using single-cell Raman spectroscopy. *Proc. Natl. Acad. Sci. U.S.A.* **108**, 3809–3814 (2011).
29. G. Azemtsop Matanfack, J. Rüger, C. Stiebing, M. Schmitt, J. Popp, Imaging the invisible-Bioorthogonal Raman probes for imaging of cells and tissues. *J. Biophotonics* **13**, e202000129 (2020).
30. J. De Gelder, K. De Gussem, P. Vandenabeele, L. Moens, Reference database of Raman spectra of biological molecules. *J. Raman Spectrosc.* **38**, 1133–1147 (2007).
31. C. Ross, K. Scherlach, F. Kloss, C. Hertweck, The molecular basis of conjugated polyyne biosynthesis in phytopathogenic bacteria. *Angew. Chem. Int. Ed. Engl.* **53**, 7794–7798 (2014).
32. N. Ziemert, M. Alanjary, T. Weber, The evolution of genome mining in microbes – A review. *Nat. Prod. Rep.* **33**, 988–1005 (2016).
33. A. J. Mullins *et al*., Exploration of polyyne biosynthetic gene cluster diversity in bacteria leads to the discovery of the *Pseudomonas* polyyne protegencin. *bioRxiv* [Preprint] (2021). https://www.biorxiv.org/content/10.1101/2021.03.05.433886v1 (Accessed 17 April 2021).
34. K. A. Hassan *et al*., Inactivation of the GacA response regulator in *Pseudomonas fluorescens* Pf-5 has far-reaching transcriptomic consequences. *Environ. Microbiol.* **12**, 899–915 (2010).
35. K. Fritsche *et al*., Biosynthetic genes and activity spectrum of antifungal polyynes from *Collimonas fungivorans* Ter331. *Environ. Microbiol.* **16**, 1334–1345 (2014).
36. K. Kai, M. Sogame, F. Sakurai, N. Nasu, M. Fujita, Collimonins A–D, unstable polyynes with antifungal or pigmentation activities from the fungus-feeding bacterium *Collimonas fungivorans* Ter331. *Org. Lett.* **20**, 3536–3540 (2018).
37. Z. P. Yordanova, E. J. Woltering, V. M. Kapchina-Toteva, E. T. Iakimova, Mastoparan-induced programmed cell death in the unicellular alga *Chlamydomonas reinhardtii*. *Ann. Bot.* **111**, 191–205 (2013).
38. S. Franz *et al*., Structure of the bifunctional cryptochrome aCRY from *Chlamydomonas reinhardtii*. *Nucleic Acids Res.* **46**, 8010–8022 (2018).
39. J. S. Boyd, T. M. Mittelmeier, M. R. Lamb, C. L. Dieckmann, Thioredoxin-family protein EYE2 and Ser/Thr kinase EYE3 play interdependent roles in eyespot assembly. *Mol. Biol. Cell* **22**, 1421–1429 (2011).
40. Q. Yan *et al*., Secondary metabolism and interspecific competition affect accumulation of spontaneous mutants in the GacS-GacA regulatory system in *Pseudomonas protegens*. *mBio* **9**, e01845-17 (2018).
41. A. L. Shi Shun, R. R. Tykwinski, Synthesis of naturally occurring polyynes. *Angew. Chem. Int. Ed.* **45**, 1034–1057 (2006).
42. K. Kai, Bioorganic chemistry of signaling molecules in microbial communication. *J. Pestic. Sci.* **44**, 200–207 (2019).
43. J. Lee *et al*., Identification of feldin, an antifungal polyyne from the beefsteak fungus *Fistulina hepatica*. *Biomolecules* **10**, 1502 (2020).
44. L. V. Flórez *et al*., Antibiotic-producing symbionts dynamically transition between plant pathogenicity and insect-defensive mutualism. *Nat. Commun.* **8**, 15172 (2017).
45. A. J. Mullins *et al*., Genome mining identifies cepacin as a plant-protective metabolite of the biopesticidal bacterium *Burkholderia ambifaria*. *Nat. Microbiol.* **4**, 996–1005 (2019).
46. W. L. Parker *et al*., Cepacin A and cepacin B, two new antibiotics produced by *Pseudomonas cepacia*. *J. Antibiot. (Tokyo)* **37**, 431–440 (1984).

47. P. Znachor, J. Jezberová, The occurrence of a bloom-forming green alga *Pleodorina indica* (Volvocales) in the downstream reach of the River Malše (Czech Republic). *Hydrobiologia* **541**, 221–228 (2005).
48. M. D. Herron, Origins of multicellular complexity: *Volvox* and the volvocine algae. *Mol. Ecol.* **25**, 1213–1223 (2016).
49. J.-D. Kim, B. Kim, C.-G. Lee, Alga-lytic activity of *Pseudomonas fluorescens* against the red tide causing marine alga *Heterosigma akashiwo* (Raphidophyceae). *Biol. Control* **41**, 296–303 (2007).
50. E. H. Harris, *The Chlamydomonas Sourcebook*, E. H. Harris, D. B. Stern, G. B. Witman, Eds. (Academic Press, London, ed. 2, 2009), vol. 1, pp. 99–103 and 241–302.
51. W. Inwood, C. Yoshihara, R. Zalpuri, K.-S. Kim, S. Kustu, The ultrastructure of a *Chlamydomonas reinhardtii* mutant strain lacking phytoene synthase resembles that of a colorless alga. *Mol. Plant* **1**, 925–937 (2008).
52. A. Ramette *et al*., *Pseudomonas protegens* sp. nov., widespread plant-protecting bacteria producing the biocontrol compounds 2,4-diacetylphloroglucinol and pyoluteorin. *Syst. Appl. Microbiol.* **34**, 180–188 (2011).
53. RCoreTeam, *R: A Language and Environment for Statistical Computing* (R Foundation for Statistical Computing, Vienna, Austria, 2020).
54. T. Bocklitz, A. Walter, K. Hartmann, P. Rösch, J. Popp, How to pre-process Raman spectra for reliable and stable models? *Anal. Chim. Acta* **704**, 47–56 (2011).
55. T. W. Bocklitz, S. Guo, O. Ryabchykov, N. Vogler, J. Popp, Raman based molecular imaging and analytics: A magic bullet for biomedical applications!? *Anal. Chem.* **88**, 133–151 (2016).
56. C. G. Ryan, E. Clayton, W. L. Griffin, S. H. Sie, D. R. Cousens, SNIP, a statistics-sensitive background treatment for the quantitative analysis of PIXE spectra in geoscience applications. *Nucl. Instrum. Methods Phys. Res. B* **34**, 396–402 (1988).